Advanced Physics Lab I

Lab Report #2 Ultrasonic Waves

Group 1
Noah Horne, Luka Burduli

23.09.2024

Dr. Veit Wagner
Tim Jesko Söcker

We hereby declare that we (Luka Burduli and Noah Horne) are the sole authors of this lab report and have not used any sources other than those listed in the bibliography and identified as references throughout the report.

_____ _____

Contents

1 Abstract

This report served as an investigation into the properties of ultrasound, and piezoelectric transducers. The bandwidth of a 40kHz transducer was measured to be $(2.8 \pm 0.02)[kHz]$ via the FWHM of its power, and $(1.9 \pm 0.02)[kHz]$ via the -3dB cutoff frequency band. The superposition of ultrasonic waves was analyzed, and beating frequencies of $(1.39 \pm 0.01)[kHz]$, $(0.53 \pm 0.01)[kHz]$, and $(0.71 \pm 0.01)[kHz]$ were measured for 2 similar amplitude wave cases and 1 different amplitude wave case respectively. The velocity of sound was measured as $(357.56 \pm 6.9)[ms^{-1}]$ and $(316.04 \pm 4.9)[ms^{-1}]$ for two distinct setups. Lastly, a table of angles to first maxima and minima for diffraction patterns was produced for slit numbers 1,2,4,6,8,10,12 and 14 accordingly.

2 Introduction and Theory

This investigation primarily focuses on the examination of the diffraction, velocity of propagation and superposition of ultrasound. The nature of ultrasonic wave transducers and their functionality is also examined through the calculation of their bandwidths–ranges of acceptable frequencies such that vibrations produced are near the resonant frequency of the piezoelectric quartz crystal.

An ultrasonic wave is classified as a sound wave whose frequencies lie outside of the upper range of human hearing ($\approx 20kHz$) (Purves, Augustine, Fitzpatrick, et al., 2001). A wave can be described formulaically as a particles' displacement over time, more specifically a function of acoustic pressure A_p over space x and time t. The solution to the wave equation:

$$\nabla^2 A_p - \frac{1}{v_s}\frac{\partial^2 A_p}{\partial t^2} = 0 \tag{1}$$

Is given by a time-position scaled sine wave with an associated amplitude A_0 and phase shift ϕ_0.

$$A_p(x,t) = A_0 \sin(\Phi(x,t)) = A_0 \sin(k \cdot x - \omega \cdot t + \phi_0) \tag{2}$$

In order to then experimentally verify the properties of this type of sound, special instruments which operate on frequencies higher than the human range of hearing must be used: piezoelectric transducers. Piezoelectric transducers are instruments that convert electrical energy into the vibrations of a piezoelectric crystal, producing ultrasonic waves due to a change in acoustic pressure around the crystal (Eq 2). As a result of the crystal warping when exposed to a charge, this process can be reversed, allowing the transducer to function as a microphone. The power of the signal produced by a piezoelectric transducer receiving an ultrasonic wave is directly proportional to the square of the amplitude of the wave ($P \propto A_p^2$)(Wagner & Söcker, 2024). Furthermore, the signal level L produced by the transducer is directly defined by the power P of the signal, where P_0 is the power measured at the transducers resonant frequency.

$$L = 10\log_{10}\left(\frac{P}{P_0}\right)[dB] \tag{3}$$

Since the square of the amplitude A_p is proportional to the power, we can substitute it in with a proportionality constant α. Note that as a ratio is taken, the constants cancel out.

$$L = 10\log_{10}\left(\frac{\alpha A_p^2}{\alpha A_0^2}\right) \implies L = 20\log_{10}\left(\frac{A_p}{A_0}\right)[dB] \tag{4}$$

As with any elastic body which can be considered non-rigid, specific resonant eigen-frequencies exist for the medium which yield much stronger vibrations. As the crystal takes on the structure of a forced-damped oscillator, there exists such an excitation frequency that exhibits resonance on the piezoelectric material. Outside of this resonant range, the observed amplitude of vibration is much less, and so, one can assign an associated bandwidth to the piezo-electric crystal and the amplitude and power of the frequencies that it produces via the FWHM of the power. Another way that we can define the bandwidth is in relation to human hearing. When a value of -3dB is reached, it is no longer perceptible to the human ear if it were an audible frequency. Using these two measurements, two associated bandwidths of the piezoelectric ultra-sonic transducer can be calculated, furthering our knowledge of our instrumentation for further experimentation.

As demonstrated earlier, a wave can be described as an oscillating sine wave with an associated amplitude A_0, phase shift, time dependent scaling and position dependent scaling (Eq 2). So, it is natural to assume that waves can superpose one another, the same way that we can simply add two solutions $(A_1(x,t), A_2(x,t))$ of the wave equation.

$$A_{superposed} = A_1(x,t) + A_2(x,t) \implies$$

$$A_{1,0}\sin(k_1 t - \omega_1 t + \phi_{1,0}) + A_{2,0}\sin(k_2 x - \omega_2 t + \phi_{2,0}) \tag{5}$$

If the two waves are of equal amplitude A_0 and both have zero phase shift ($\phi_{1,0} = \phi_{2,0} = 0$), one can substitute and simplify such that the resultant superposed wave is written as:

$$A_{superposed} = 2A_0\cos(2\pi\frac{f_1 - f_2}{2}t)\sin(2\pi\frac{f_1 + f_2}{2}t) \tag{6}$$

where f_1 and f_2 are the frequencies of the waves 1 and 2 respectively. It is clear that there are two frequencies in consideration here. One frequency is equivalent to the beating frequency f_b observed by the difference in frequency between the two waves (inside of the cos term), and the other is equivalent to the carrier frequency f_m, which is the mean of the two frequencies (inside of the sin term). To determine the values of the beating frequency experimentally, the beating period is determined, and from that, the frequency f_b is derived.

$$T_p = \frac{1}{f_b} \tag{7}$$

Due to ultrasonic waves penetrating power, they are used extensively in fields such as medicine and ocean topography. More specifically, in ocean topograpohy ultrasonic transducers are used as a means of finding the distance to the bottom of the ocean without physical measurement. By simply knowing the velocity of propagation v_s of ultrasound through the seawater, an ultrasonic depth finder calculated the distance Δs to the sea floor by measuring the time required for an ultrasonic wave to reflect off the sea floor and return to the tranduser. The distance is then calculated using the following formula:

$$\Delta s = v_s \cdot \Delta t \tag{8}$$

The depth to the ocean floor is then simply found by halving the calculated Δs. Reverse engineering this process, one can experimentally determine the speed of sound by simply calculating the proportional relationship between half the distance travelled by a reflected ultrasonic wave in air, and the time taken for it to propagate.

$$v_s = \frac{\Delta s}{2 \cdot \Delta t} \tag{9}$$

Lastly, as ultrasonic waves are still sound waves nonetheless, they are subject to diffraction in a similar way. For a sound wave travelling through a *single slit*, the destructive and constructive interference forms a pattern of maxima and minima. The angle to the first minima of a single slit pattern is given by:

$$\sin \theta_k = \frac{\lambda}{b} \tag{10}$$

where b is the width of the slit, and lambda is the wavelength. As for systems with multiple slits, the angle to the kth maxima of the diffraction pattern is given by a similar formula, only this time characterized by the distance between slits d rather than slit width.

$$\sin \theta_k = \frac{k\lambda}{d} \tag{11}$$

With the relevant theory established, the investigation can be conducted empirically, and theoretical calculations can be used to ensure the validity of the data produced.

3 Experimental Procedure

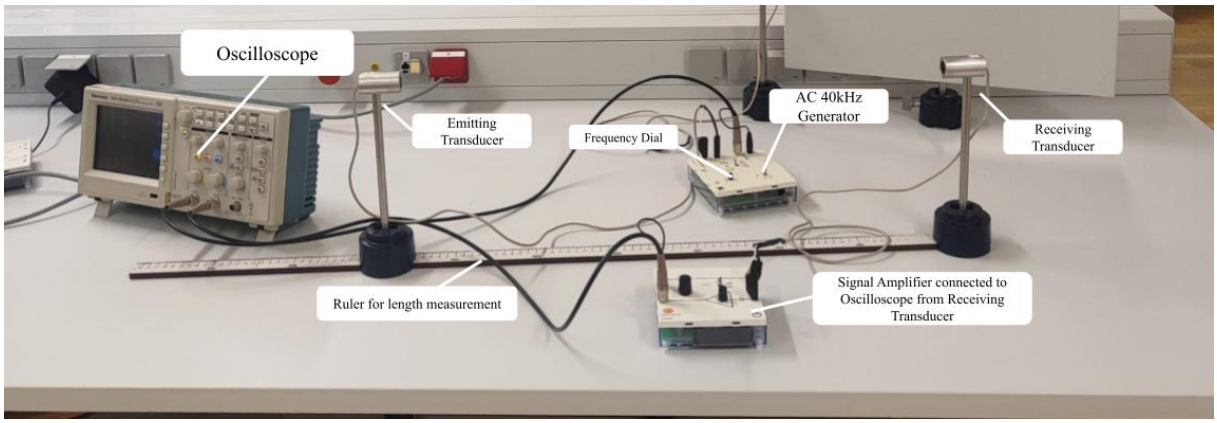

Figure 1: Experimental Setup for the Bandwidth Calculation of a Piezoelectric Transducer

As aforementioned, this investigation focues primarily on the investigation of the properties of ultrasonic waves and the intruments that produce them.

For the first part of the experiment, the bandwidth of a piezoelectric ultrasonic tranducer is measured. The setup involves two transducers. One trandsucer is responsible for the emmission of ultrasonic waves at varying frequencies. It is connected to a 40kHz AC generator which produces an alternating current running through the piezoelectric, producing ultrasonic waves of the given AC frequency. To measure these waves, another receiving transducer is positioned diametrically opposed to the emmitter and connected to a signal amplifier to compensate for any loss in amplitude due to the acoustic impedance in the air. The signal is then visualized and measured using an oscilloscope as seen in Figure 1.

First, the resonant frequency is measured by manually altering the frequeny dial on the amplifier until a maximum amplitude is observed on the oscilloscope. After this value is measured, the frequency is varied as high as it can still be properly measured, by the oscilloscope and then decremented slowly to observe the relationship between frequency and amplitude, read off of the oscilloscope. Plotting this data and determining the FWHM the bandwidth is determined. Furthermore, by converting the collected data from amplitude to signal level $[dB]$ using formula 4, the -3dB threshold width can be determined as well. As a note, sometimes in the data collected there are an insufficient number of points close to the area of interest we are looking for (-3dB). To correctly determine the frequeny values which would sit at a signal level of -3dB, an interpolation of the data points was performed, allowing one to find any point needed along the curve.

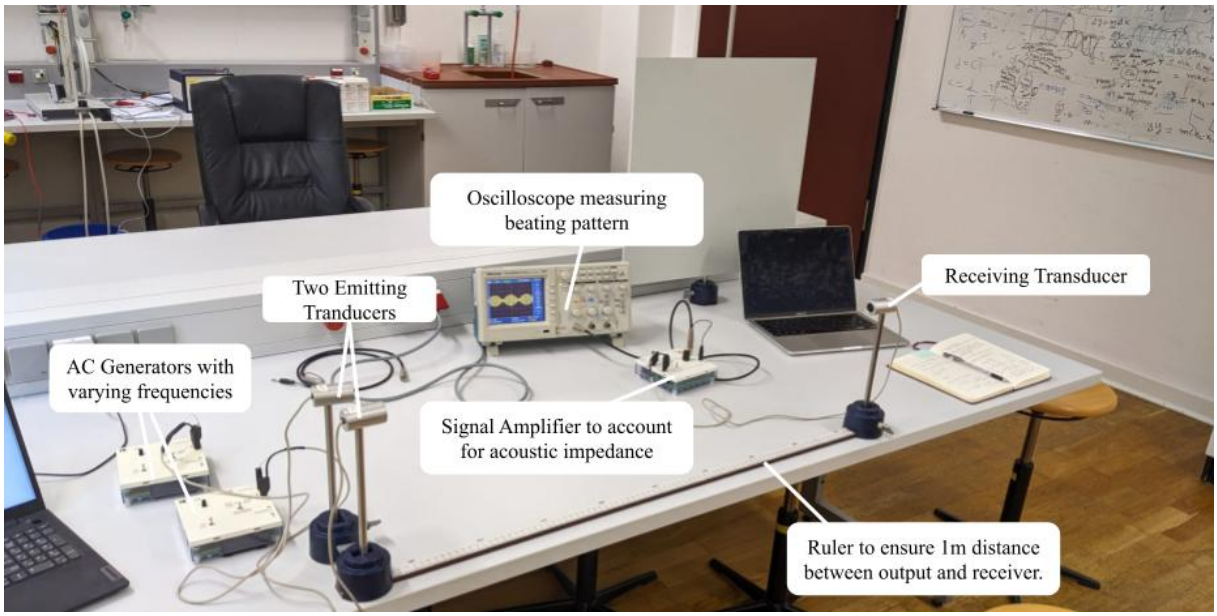

Figure 2: Experimental Setup for the Measurement of the Beating Frequency

It is known that two similar amplitude sound waves travelling with relative zero phase difference will constructively and destructively interfere with one another, creating a beating pattern. This beating pattern is formulaically described by equation 6, and as mentioned, gives rise to two frequencies: the carrier frequency f_m, and the beating frequency f_b. Using the inner consituents in the sine and cosine terms of superposed amplitude function, $f_b = \frac{f_1 - f_2}{2}$ and $f_m = \frac{f_1 + f_2}{2}$, one calculates the theoretical beating frequency. To empirically measure the beating frequency, one first ensures that both transducers are of equal amplitude and different frequency (marking them down). After each amplitude is measured individually and it is assumed that they are equal, both emitters are turned on. In order to observe a nice beating pattern, only one of the transducers frequencies is slightly varied until a clear beating pattern accors. Then, one simply uses the markers on the oscilloscope to measure the period T_b, applying formula 7 for the frequency. After the measrurements, only the transducer with responsible for fine tuning the beating is left on, so that its new frequency can be used for theoretical calculations. After the relationship between the beating frequency of similar amplitude waves is measured, one transitions to varied amplitude measurements.

This switch in setup is relatively straightforward. One simply sets one of the transducers to emit sound with 2/3 the amplitude of the resonant frequency, and the other transducer to emit sound at 1/2 of its resonant frequency, ensuring a difference in amplitude. These measurements are noted down, and then the same measurements as before are taken for the beating frequency, the carrier frequency, and the amplitude of the resultant superposed wave.

For the calculation of the velocity of ultrasound, the same methods employed in ocean topography were used. One simply uses two transducers–one emitting, one receiving– diametrically opposed to an acoustic reflecting plate.

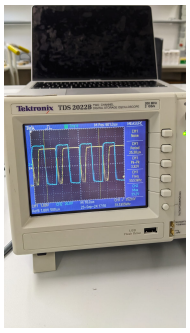

Figure 3: Oscilloscope view of shift between emitted (blue) and received (yellow) signal.

By measuring the distance between the transducers and the reflecting plate, comparing the time difference between the pulses sent by the emitter and received by the receiver, the time taken for the wave to propagate the entire distance is calculated (See Figure 3). Using this time, it was plotted for various distances to the acoustic reflecting plate to create a linear relationship. From this, the slope of the graph of the distance to the acoustic reflecting plate directly reads off the velocity of sound in air. After this is complete, the acoustic plate is then removed and replaced with a transducer. The velocity of sound is then measured without the use of a reflecting plate by replacing the plate with another transducer. The velocity of sound is then measured without reflection in a similar manner.

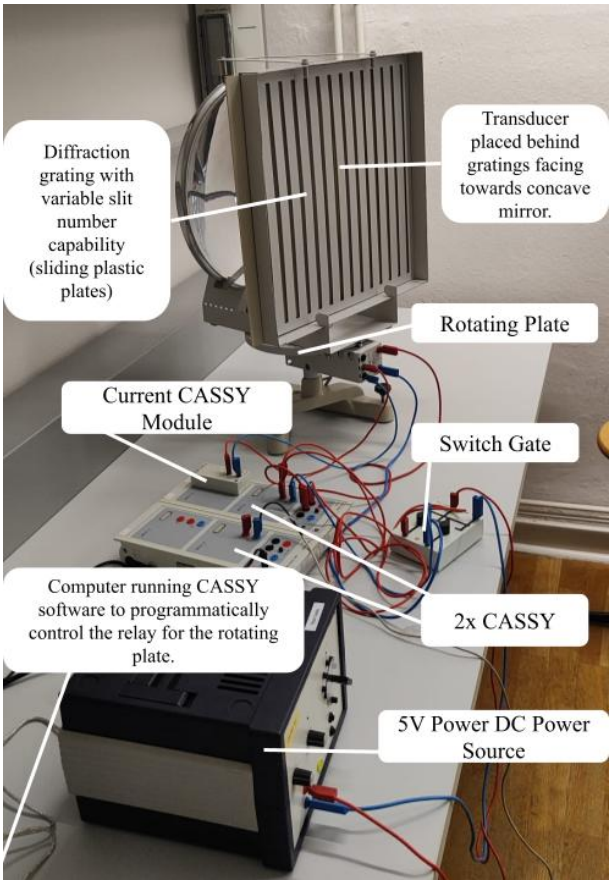

Figure 4: Setup for measurement of diffraction pattern for varying number of slits

The last aspect of this investigation focuses on the measurement of the diffraction pattern of ultrasound as a means of verifying the diffractive behavior of ultrasound, and calculating the angle to the first maxima and minima formed by slits through which the ultrasonic waves pass. The angle in radians to the first maxima, from a theoretical standpoint, is given by formula 11. One can first theoretically calculate the expected value one should obtain from performing this experiment, and then do so experimentally.

For this setup, a rotating plate is used to rotate an entire setup between -90^o to 90^o. Placed on the rotating plate is a piezoelectric transducer emitted into a concave reflecting plate, which centers the sound waves onto slits positioned behind the transudcer. As the ultrasonic waves pass through the slits, a diffraction pattern is created. 5 meters away from the rotating setup, a single receiver transducer is positioned. This transducer is connected to a signal amplifier which runs directly into the cassy where the RMS AC amplitude is measured and plotted as a function of angle. As the setup rotates, so does the entire interference pattern, allowing the receiver transducer to take a codimension one cross section of the interference pattern for many many angles, yielding the interference pattern of the ultrasound.

To measure the angle rotated through by the plate, the resistance of a angular potentiometer is measured and transfered through a CASSY. In order to first establish a relationship between the resistance observed and the angle rotated, a coefficient must be determined. To do this, a plot of the resistance against angle is created, and the slope noted down. This slope serves as a 'translator' between the incoming resistance values to the CASSY, and the outputted angle values which are necessary for proper calculations. For all further measurements, the RMS power is plotted against the angle of the setup. Measurements of the diffraction patterns were taken for 1,2,4,6,8,10,12 and 14 slits respectively. The minima of the single slit being measured, and the maxima of the multi slit patterns measured.

4 Results and Data Analysis

To begin, the bandwidth of a piezoelectric ultrasonic transducer was determined. First, the values of the resonant frequency were found by manually varying the amplitude to find the frequency that yielded the largest amplitude on the oscilloscope. The values found for the resonant frequency f_r and maximum amplitude A_{max} were:

$$f_r = (40.39 \pm 0.01) \quad [kHz]$$

$$A_{max} = (2.26 \pm 0.01) \quad [V]$$

These values will be used later as a means of normalizing the data for a more efficient calculation of the bandwidth. Below denotes the table of raw data measured for the amplitude received by the diametrically opposed piezoelectric transducer and the frequency emitted.

Table 1: Frequency of Ultrasonic Wave against Amplitude and Signal Level Observed			
Frequency (kHz) +- 0.01kHz	Amplitude (V) ±0.01 (V)	Signal Level (dB)	Propagated Error for Signal Level (dB)
39.22	1.15	-5.87	0.21
39.4	1.45	-3.85	0.15
39.5	1.52	-3.45	0.13
40.13	2.2	-0.23	0.03
40.39	2.26	0	0
40.76	2.22	-0.156	0.023
41.1	1.94	-1.33	0.073
41.5	1.49	-3.62	0.14
42.02	1.15	-5.87	0.21
42.37	0.9	-7.99	0.28
42.94	0.68	-10.43	0.39

The light green highlighted cells denote the resonant frequency f_r and maximum amplitude A_{max} of the the transducer, whereas the darker green indicate the frequency and amplitude values corresponding to the closest data point to the FWHM defining data. Below are the two plots that visually represent this data. The lines were used to determine the FWHM and the -3dB threshold value. Notice also that the signal level is normalized from zero at the maximum amplitude.

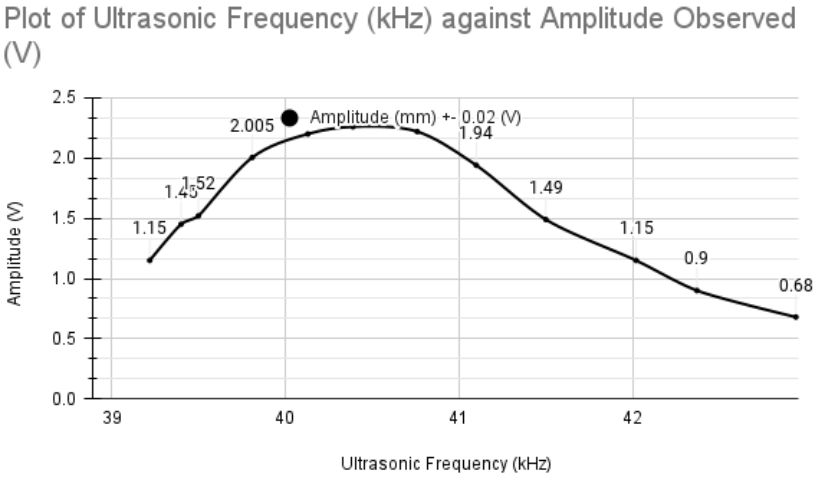

Figure 5: Plot of Ultrasonic Frequency (kHz) against measured Amplitude (V)

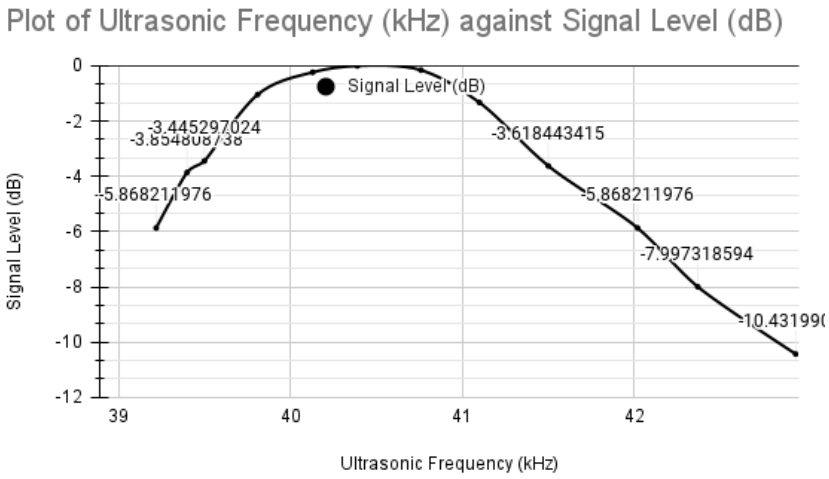

Figure 6: Plot of Ultrasonic Frequency against Signal Level (dB)

From these two graphs, the full width half maximum (FWHM) and the -3dB threshold values were calculated as measurements for the bandwidth of the piezoelectric transducer. Below denotes the final calculated values extracted from the data above. For the two values used in the calculation of the -3db frequency bandwidth, the interpolated values from the graph were used as the data set was did not provide sufficiently close measurements to use.

$$\text{Maximum Amplitude } A_{max} = (2.26 \pm 0.01)V$$

$$\text{Half Amplitude } \frac{A_{max}}{2} = (1.13 \pm 0.005)V$$

$$\text{FWHM Value} = 42.02[kHz] - 39.22[kHz] = \underline{(2.8 \pm 0.02)[kHz]}$$

$$\text{-3dB Frequency Bandwidth} = 41.42292[kHz] - 39.51833[kHz] = \underline{(1.9 \pm 0.02)[kHz]}$$

The data above clearly demonstrates the force-damped harmonic oscillator like nature of the piezoelectric crystal in the transducer, as a clear resonant frequency and rapid decay is observed from the graphs. The two different bandwidths demonstrate two distinct measures for cutoff frequencies–one related to the human perception of sound, and the other related to the amplitude measured by the oscilloscope. As a takeaway, both measurements give a strong idea of the sensitive frequency requirements necessary for ultrasound piezoelectric transducers to produce an optimal amplitude. Therefore, when using such transducers in real world applications, it is crucial that the resonant frequency of the piezoelectric element is considered to ensure optimal functionality.

The next part of this investigation focuses on the superposition of two ultrasonic waves. First, the beating frequency of two ultrasonic waves of the same amplitude is measured two times. The first time, both values are half of their maximum amplitudes. The second time, both values are one third of their maximum amplitudes. Next, the same measurements are taken, only for

differing amplitudes of 2/3 and 1/2 the max. amplitude A_{max}. Below is the table of all values collected for first each amplitude and frequency measured indiviually, then measured together, and then only the frequency of the slightly modified tranducer to ensure clear peak behavior.

Table 2: Amplitude, Measured Frequency and Beating Frequency with 1/2 Max Amplitude (V)					
Transducers	Transducer A	Transducer B	Transducer A&B		Transducer B
Max Amplitude/2 (V)	1.015±0.005	1,015±0.005	1.4±0.005		0.85±0.005
Measured Frequency (kHz)	39.09±0.01	40.50±0.01	Carrier Freq: 40.11±0.01	Beating Freq: 1.39±0.01	41.9±0.01

Table 3: Amplitude, Measured Frequency and Beating Frequency with 1/3 Max Amplitude (V)					
Transducers	Transducer A	Transducer B	Transducer A&B		Transducer B
Max Amplitude/3 (V)	0.77±0.003	0.77±0.003	1.15±0.003		0.77±0.003
Measured Frequency (kHz)	39,09±0.01	40.50±0.01	Carrier Frequency: 39.47±0.01	Beating Frequency: 0.53 ±0.01	41.9±0.01

To ensure the scientific accuracy of the data from the tables above, it is crucial to compare to theoretical values. It is clear that the idea of amplitude superposition holds, in that the maximum amplitude of both A and B is approximately the sum of the two individual amplitudes combined. Furthermore, by using the theory developed by formula 6, one can easily arrive at formulas for the beating frequency f_b and the carrier frequency f_m of the superposed wave.

$$f_b = \frac{f_2 - f_1}{2}, \qquad f_m = \frac{f_2 + f_1}{2} \tag{12}$$

As a sample calculation, the beating frequency and carrier frequency of the interered wave formed by two waves of 1/2 the maximum amplitude A_{max} will be calculated.

$$f_b = \frac{f_2 - f_1}{2} = \frac{41.9[kHz] - 39.05[kHz]}{2} = \underline{(1.43 \pm 0.01)[kHz]}$$

$$f_m = \frac{f_2 + f_1}{2} = \frac{41.9[kHz] + 39.05[kHz]}{2} = \underline{(40.48 \pm 0.01)[kHz]}$$

Following this process the comparative table below was constructed for both of the similar amplitude setups ($\frac{1}{2}A_{max}$, $\frac{1}{3}A_{max}$).

Table 4: Comparison between Theoretical and Empirical data for f_b and f_m				
	$\frac{1}{2}A_{max}$ Comparison		$\frac{1}{3}A_{max}$ Comparison	
	Carrier Frequency (kHz)	Beating Frequency (kHz)	Carrier Frequency (kHz)	Beating Frequency (kHz)
Measured Value	40.11±0.01	1.39±0.01	39.47±0.01	0.53±0.01
Theoretical Value	40.48±0.01	1.43±0.01	39.48±0.01	0.58±0.01

The data above suggests a commendable degree of accuracy between the theoretical values of the frequencies and the measured values. While some error persists in the measurements, most notably for the carrier frequency of the wave composed of two $\frac{1}{2}A_{max}$ amplitudes, this is likely due to atmospheric causes in the experimental room which altered the final measured result (temperature, humiditiy, and the acoustic impedance of air).

While the data above confirms the theory developed for the interference of two similar amplitude waves, the superposition of two different amplitude waves has yet to be examined. Below denotes the table of raw data containing the measurements of the individual frequencies A and B, and the carrier and beating frequency of the superposed wave. Note that first the transducers were adjusted to emit their resonant frequency (the values noted down), and then modified to produce the altered lower amplitude.

Table 4: Amplitude, Measured Frequency and Beating Frequency with two waves of different amplitude						
	Tranducer A		Tranducer B		Traducer A&B	Tranducer B
Maximum Amplitude (V)	2.3±0.02	Maximum Amplitude (V)	2.04±0.02			
Frequency of Max. Amplitude (kHz)	40.403±0.01	Frequency of Max. Amplitude (kHz)	40.934±0.01			
2/3 Max. Amplitude (V)	1.53±0.01	1/3 Max Amplitude (V)	0.68±0.01	Max Amplitude (V)	2.24±0.01	1.28±0.01
Measured Frequency (kHz)	39.3±0.01	Measured Frequency (kHz)	38.38±0.01	Carrier Frequency (f_m) (kHz)	39.91±0.01	40.82±0.01

The table above represents the amplitude, carrier frequency, and beating frequency of the superposition of the two waves with different amplitudes (2/3 and 1/3 of their maximum). Extracting the data from the table confirms the theory of constructive interference–the resultant amplitude of two waves of differing amplitudes (2.24±0.01)[v] is very close to the sum of both wave's amplitudes combined: 1.53[V]+0.68[v]=(2.21±0.02)[v]. As $2.24 \pm 0.01 \approx 2.21 \pm 0.02$, since they just barely fall into each others error, one can sufficiently confirm that the measured raw data values are indeed consistent with the theory. Furthermore, using the same exact calculation method as detailed earlier to compute the theoretical values of the carrier and beating frequency, the table below compares the two results.

Table 5: Comparison between Theoretical and Empirical data for f_b and f_m for different Amplitude		
	Experimentally measured data	Theoretical Value
f_m (kHz):	39.91±0.01	40.06±0.01
f_b beating frequency (kHz):	0.71±0.01	0.76±0.01

While the measured values and the theoretical values do not fall between each others error, they are very closely correlated. This slight deviation is expected due to the real world conditions and random sources of error present, as aforementioned. However, the properties of wave superposition were successfully verified from this data due to the observed similarities between the measured values and the theoretical values.

In the next part of the experiment, the time difference between the emitted and received ultrasonic pulses for various distances from the acoustic reflecting plate was measured. The collected data is summarized in Table 6 below:

Table 6: Measurement of distance and time for Propagation with Acoustic Reflector		
time (±0.01)($10^{-3}s$)	distance (±0.001) (m)	$2 \cdot$ distance (±0.002) (m)
3.54	0.6	1.2
3.2	0.55	1.1
3	0.5	1
2.72	0.45	0.9
2.4	0.4	0.8
2.12	0.35	0.7
1.76	0.3	0.6
1.52	0.25	0.5
1.28	0.2	0.4
0.96	0.15	0.3
0.84	0.1	0.2

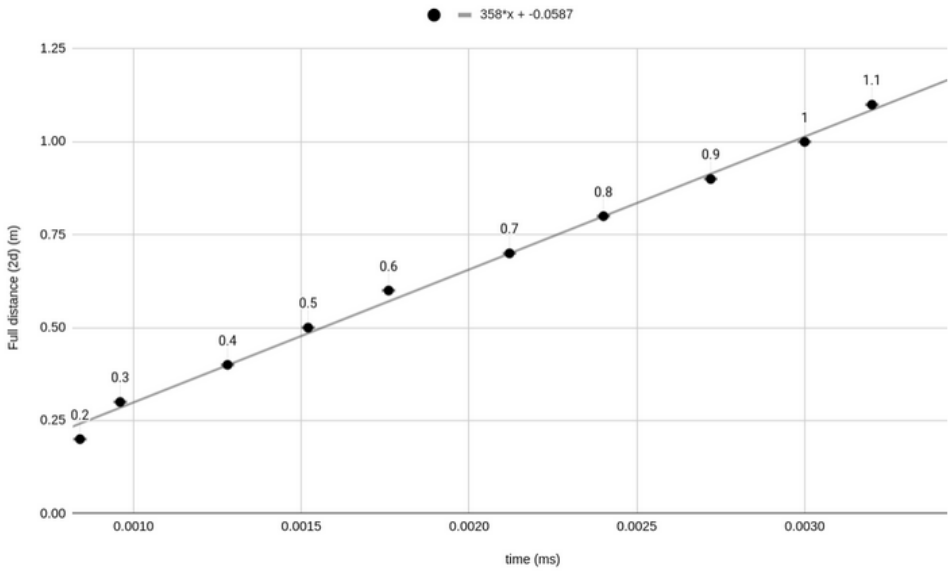

Figure 7: Plot of 2·Distance Between the Transducer and Acoustic Reflector against Time

Using these measurements, a plot of $2 \cdot$ Distance (m) versus Time (ms) was created. The slope of the linear regression line through these data points represents the measured velocity of sound. The obtained slope was 357.56 m/s, with an error calculated by the least squares method (LINEST) of ±6.94 m/s. As aforementioned, the slope can then be considered the directly measured value of the velocity of sound using this method, as the scaling of the distance already took place. Therefore, the calculated velocity of sound found through the use of a diametrically opposed acoustic reflecting plate is:

$$v_{plate} = (357.56 \pm 6.9)[ms^{-1}]$$

Table 7: Measurement of distance and time for Propagation without Acoustic Reflector	
Time ±0.01 (10^-3) s	Distance Travelled (m)
2.20	0.65
2.00	0.60
1.84	0.55
1.72	0.50
1.52	0.45
1.36	0.40
1.24	0.35
1.04	0.30
0.92	0.25
0.70	0.20
0.64	0.15
0.44	0.10

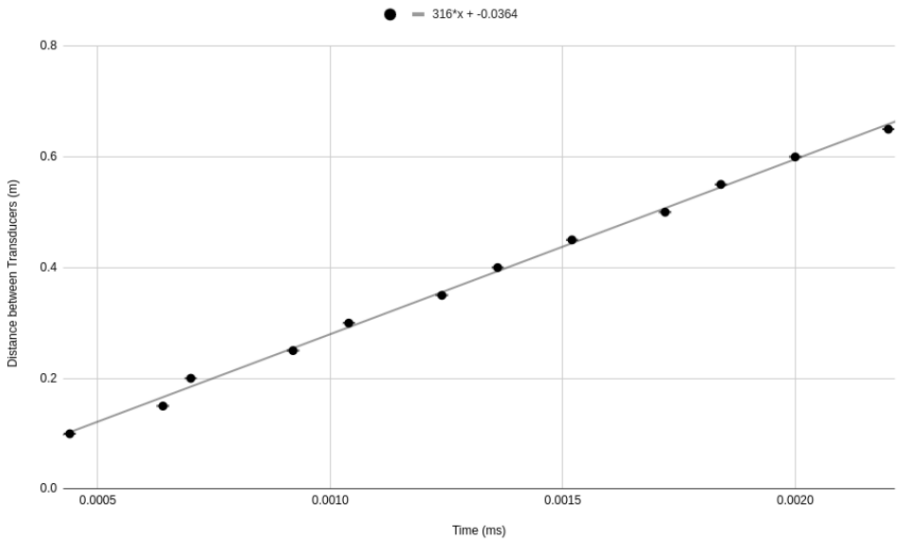

Figure 8: Plot of 2·Distance Between the Transducer and Acoustic Reflector against Time

The slope of the linear regression line through these data points represents the measured velocity of sound. The obtained slope was (316.04 ±4.88)m/s, with an error similarly calculated via the least squares method (LINEST). Therefore, the calculated value of the velocity of sound was also:

$$v_s = (316.04 \pm 4.9)x[ms^{-1}]$$

These results demonstrate a clear difference in the measured velocities, which can be attributed to several factors including potential differences in the experimental setup, measurement precision, and environmental conditions.The expected velocity of sound in air at room temperature (20°C) is approximately 343 m/s (OpenStax, 2024). The value obtained with the acoustic reflector

(357.56 m/s) is closer to this expected value compared to the value obtained without the reflector (316.04 m/s). This is likely due to the fact that the sound has the chance to travel through more air (twice the distance) using the reflector, which allows for any random error produced by atmospheric effects to be averaged out over a longer period, producing less sporadic data.

The next part of the experiment was about exploring the relationship between the resistance and the angle of a rotary stage. By analyzing this relationship, a coefficient was determined to translate between the resistance data and the angle of the rotary stage, which was used later to study the behaviour of light diffraction for a varying number of slits. Below denotes the table of measurements relating the angle of the rotary stage (observed visually) and the resistance measured by the CASSY.

Table 8: Angle (degrees) of rotary table against Resistance (kilo ohms)

Angle ±0.05 (Degrees)	Resistance ±0.01 (kOhm)
-90	7.30
-80	7.05
-70	6.80
-60	6.54
-50	6.28
-40	6.03
-30	5.78
-20	5.53
-10	5.27
0	5.00
10	4.76
20	4.49
30	4.24
40	3.97
50	3.70
60	3.45
70	3.22
80	2.95
90	2.71

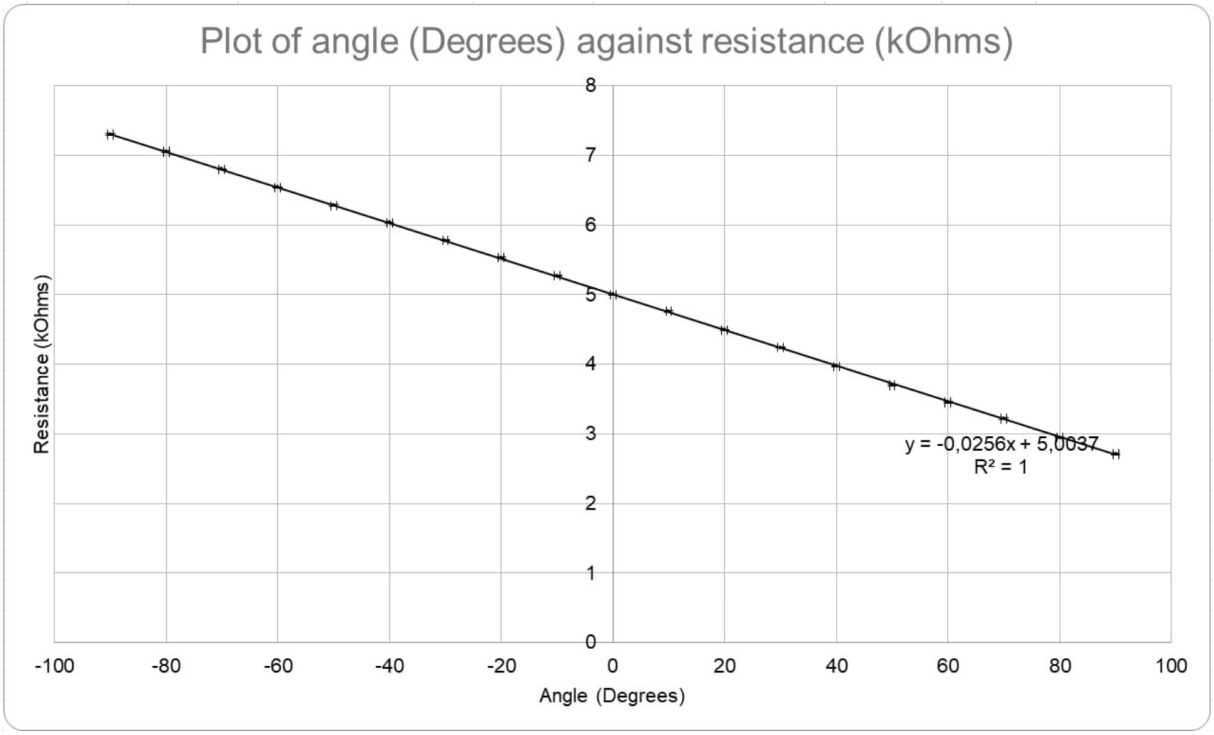

Figure 9: Angle of Rotary Stage (Degrees) Against Resistance (kOhms)

The data from the graph suggests that there is a very strong negative linear correlation between the resistance R and the angle θ, which can be expressed in terms of the resistance R via the relationship $\theta \approx 5 - \frac{R}{0.0256}$. By converting the resistance to angle it is possible to control rotation angle of the rotary stage automatically by measuring the angle through the CASSY–with the newly defined relationship–and set constraints for the angle through which the rotary plate moves through. The following logical expression was programmed into the CASSY software using our newly defined parameter θ to define the boundaries of rotation for the rotary stage:

$$(\theta > -90) \text{ and } (\theta < 90)$$

Using this newly defined parameter, the diffraction pattern of ultrasound was measured automatically for a varied number of slits. The raw data collected for each of these slits can be seen displayed graphically in Appendix A. From each of these graphs, the defining features of the diffraction patterns were measured. These defining features were the angle to the first maxima for multi-slit diffraction pattern, and the angle to the first minima for the single slit diffraction pattern.

Table 9: Measured Values for the Angles (degrees) of diffraction pattern for varying numbers of slits							
number of slits:	14	12	10	8	6	4	2
Angle of Central Maximum:	0	0	0	0	0	0	0
Angle of +1 peak (± 0.01)	16.79	16.992	17.38	17.38	17.57	17.57	18.23
Angle of -1 peak (± 0.01)	-16.99	-15.23	-14.84	-15.23	-14.84	-14.64	-15.625
Angle of +2 peak (± 0.01)	34.96	35.936	35.9375	36.32	35.54	34.179	38.085
Angle of -2 peak (± 0.01)	-33.98	-32.03	-32.617	-32.617	-32	-31.05	-33.59375
Angle of +3 peak (± 0.01)	58.339	60.935	59.1796	58.98	58.78	57.42	55.46
Angle of -3 peak (± 0.01)	-57.42	-54.88	-54.2968	-48.632	-52	-55.07	-52.929

Above are the measured values for the angles of the first maxima for multi-slit diffraction patterns. Using formula 11, one can also theoretically determine the angles of the maxima for multiple slits. The distance between slits was measured to be $(0.03 \pm 0.001)m$ and the wavelength was derived from the frequency used as $0.0084m$. Using these values substituted into the formula below, the theoretical values were calculated.

Table 10: Calculated Theoretical Values for the Angles (degrees) of diffraction pattern for varying numbers of slits							
number of slits:	14	12	10	8	6	4	2
Angle of Central Maximum:	0.00	0.00	0.00	0.00	0.00	0.00	0.00
Angle of +1 peak (± 0.01)	16.26	16.26	16.26	16.26	16.26	16.26	16.26
Angle of -1 peak (± 0.01)	-16.26	-16.26	-16.26	-16.26	-16.26	-16.26	-16.26
Angle of +2 peak (± 0.01)	34.06	34.06	34.06	34.06	34.06	34.06	34.06
Angle of -2 peak (± 0.01)	-34.06	-34.06	-34.06	-34.06	-34.06	-34.06	-34.06
Angle of +3 peak (± 0.01)	57.16	57.16	57.16	57.16	57.16	57.16	57.16
Angle of -3 peak (± 0.01)	-57.16	-57.16	-57.16	-57.16	-57.16	-57.16	-57.16

As for the angle of the minima for the first slit, the comparison between the measured value and the calculated theoretical value is denoted below:

Table 11: Calculated vs. Theoretical Value of Angle to First Minima of Single Slit	
Measured Values (Degrees) ± 1 Degree	Theoretical Values (Degrees) ± 0.01 Degrees
52	57.16
-48	-57.16

The data above highlights the slight error and disparity between the measured values and the theoretical values of the angle. This can be explained immediately by observing the graphs of raw data (see Appendix A), due to the sheer quanityt of noise making it difficult to obtain accurate measurements. One thing that is quite clear is that the angle to the first minima of the single slit diffraction pattern is much larger than that to the first maxima of the multi slit pattern. However, it is interesting to note that the third maxima of the multislit pattern is directly equivalen to the first minima of the single slit, highlighting the idea of a single slit diffraction pattern envelope near the third slit.

5 Error Analysis

This investigation was subject to large amounts of error due to the variange in atmospheric conditions in the room, sensitive instruments which used amplified signals, and the extremely precise measurements needed to be made (on the order of miliseconds and kilo Hertz).

For all errors involving the slope of the graph, the uncertainty of the slope was approximated using the built-in function (LINEST), which works by approximating the linear slope of a set of data points through the least squares method. As a byproduct, the error of the slope is given in absolute form. Due to the efficiency of this method, and the large quantity of graphs, it was the clear choice for this investigation.

For all errors involving numerical calculations with propagated error, such as for the uncertainties of the final measurements, the root sum of squares method (RSS) was employed. This method involves calculating the propagated error of a formulaic value by computing all partial derivatives with respect to all error prone parameters, and taking it under a square root. The formula for this is given below.

$$\Delta y = \sqrt{\sum_{i=0}^{n} \left(\frac{\partial y}{\partial x_i} \cdot \Delta x_i \right)^2} = \sqrt{\left(\frac{\partial y}{\partial x_1} \cdot \Delta x_1 \right)^2 + \cdots + \left(\frac{\partial y}{\partial x_n} \cdot \Delta x_n \right)^2} \tag{13}$$

This formula was used to calculate the propagated error of tehe beating frequency and the carrier frequency, alongside the error of the angle for the diffraction patterns.

Moving on, one can examine more closely the error observed throughout the investigation to comment on the reliability and theoretical accuracy of the data collected. For the first aspect of the experiment, determining the resonant frequency of the ultrasonic transducer, the error achieved was commendable. As one can see, the error for the FWHM and -3dB bandwidth was $0.02[kHz]$, which only made up approximately 1% of each measured value, indicating very precise instrumentation.

Later on, the beating frequency and carrier frequency of the superposed waves was examined. It is clear comparing the measured value and the calculated value that a clear consistency with theory is present. However, the measured value does not fall sufficiently close the the theoretical value–their errors do not coincide (see Table 5). While close to one another, they do not fall in the same range. This is likely due to the random error introduced by several factors throughout the investigation–temperature fluctuation, humidity variation, and amplification noise which prevent precise measurement of the nodes in the interference pattern. Nonetheless, the data is very clearly consistent with the theory, as no major disparity between the theoretical and measured values were present.

Moving on, the velocity of sound was measured in two different ways, each with it's own associated error. When using the acoustic plate, the value for the velocity of sound was calculated as $(357.56 \pm 6.9)[ms^{-1}]$. When not using an acoustic plate and simply replacing it

with another transducer to measure the phase difference, the velocity of sound was calculated to be $(316.04 \pm 4.9)[ms^{-1}]$. As aforementioned, the literature value for the velocity of sound in air at 20 degrees Celsius is approximately 343 ms^{-1}(OpenStax, 2024). Comparing both results to the literature value, it is clear that the value obtained by the acoustic reflecting plate method was more literarily accurate (close to the value), however less instrumentally precise. Contrarily, the value obtained without the acoustic reflecting plate was less literarily accurate, but more instrumentally precise. This can be attributed to several reasons. First, the acoustic reference plate setup propagates the ultrasound waves through twice the distance of the setup using no acoustic reference plate. This increased distance allows for the atmospheric changes to average out over the distance, but also leads to more instrumental error. For the shorter distance of the setup without an acoustic reflecting plate, there is less time and distance for the velocity of sound to be skewed by atmospheric conditions, but any that do arise would have a more significant systematic effect. For this reason, we observe the trends mentioned above. Overall, the data collected is not fully adherent to the literature value, however can be explained through the condition in which the experiment was performed.

Lastly, one can also discuss the aspect of the investigation with the most random error, as seen graphically in Appendix A. Due to the extremely large distance between the diffraction grating and the receiving transducer, the acoustic impedance, noise from the very strong amplification, and various other environmental effect caused the data collected to be very noise-ridden and difficult to quantitatively measure. Despite these difficulties in the lab, many precautions were taken in an attempt to minimize this error and the values collected were the most optimized possible. Comparing the table of measured values (table 9) to the table of theoretical values (table 10) for the angles to the first maxima, the data collected, although slightly variant, is similar to what is expected from the relevant theory (see Formula 11). While the instrumental error for the angle in itself was not very large, the random error present was dominant and clearly fluctuated the measured values from what was expected. Additionally, due to the extremely large distance ($\approx 5m$) between the diffraction grating and the receiver, the signal was very impeded by the time it reached the receiver, and therefor had to be amplified, introducing a large amount of noise–as seen in Appendix A. Despite these error sources, a commendable degree of accuracy was obtained between the theoretical and measured values, no data point ever varying from the theoretical by more than ≈ 6 degrees.

6 Discussion

In all aspects of the investigation, it is appropriate to state that although the data measured and obtained during throughout the experimental method is sufficiently *consistent* with the relevant theory in all aspects, it still lacks the accuracy and precision required to make a more concrete and definitive judgment. Namely, the data collected for the velocity of sound, and the first maxima and minima of the diffraction patterns is cohesive–in that it demonstrates the properties of the

relevant theory–but lacks in the quality of measurement and precision required to make ones own argument.

Immediately, 3 main improvements can be made which are applicable to many aspects of the experimental procedure and are relevant in almost all parts of the investigation.

Firstly, one of the largest causes of deviation from the expected measurements is random error introduced via the temperature of the air during the experiment. The procedure used fails to acknowledge the critical importance of the temperature, humidity, and overall condition of the medium through which the ultrasonic waves propagate. The importance of the medium by which an sound wave propagates can be directly shown through the following formula, which describes the velocity of sound dependent on the medium through which it travels:

$$v = \sqrt{\frac{\gamma R T_k}{M}} \tag{14}$$

In formula 14, γ represents the adiabatic index of the ideal gas that a sound wave travels through, R being the ideal gas constant, M being the molecular mass of the medium and T_k being the absolute temperature of the gas. The reason this relationship is crucial to consider, is because it gives rise to the need to maintain a constant temperature in the room. While not immediate and sporadic in effect, closing a window during the length of the investigation after measuring base values could significantly systematically change the measured values from the theoretical prediction. To fix this in the future, a temperature controlled environment should be considered.

Second, the random noise introduced by the amplifier–an instrument present in almost all aspects of the experiment–led to many issues in maintaining accurate values, especially during the diffraction setup. To account and correct this, the whole setup should be scaled down to minimize the amount of air travelled through by the sound, and the slit distance should be decreased to allow for a more dramatic diffraction pattern to be observed, easier for instruments to pick up.

Lastly, but also very importantly, it was difficult during the experiment to properly modify the frequency in a controlled manner due to the sensitive dependence of the frequency emitted by the AC 40kHz generator and the rotation the frequency knob. During the experiment, one would simply press down on the knob slightly, and the frequency value would shift on the order of 1-2 kHz, without any rotation. This made it extremely difficult to take precise measurements simply due to this instrumental limitation. In future experiments, it would be beneficial to include a less sensitive frequency modification knob to allow for less fluctuatory frequencies and more precise values to be measured.

7 Conclusion

From the values obtained for the bandwidth of piezoelectric ultrasonic transducer, it is appropriate to conclude that there exists a very sensitive dependent between the frequency used, and the amplitude emitted by the transducer:

$$\text{FWHM Value } = (2.8 \pm 0.02)[kHz]$$

$$\text{-3dB Frequency Bandwidth } = (1.9 \pm 0.02)[kHz]$$

Considering the fact that the emitted frequency of the ultrasonic transducer for these measurements was approximately $40.39[kHz]$, such instruments involving piezoelectric materials as a method of producing ultrasonic waves are very dependent on the frequency used. As ultrasound is widely used in many fields, and transducers such as these are everywhere in modern technology, it is crucial to apply these results, and ensure that the resonant frequency of the piezoelectric element is always used to maximize the efficiency of the transducer.

Moving on, the results obtained for the superposition of two waves of similar and of difference amplitude demonstrates a phenomena exploited by many musicians and electrical engineers alike. It is clear from the measurements that the data collected strongly adheres to the theoretical predicted values. The final values of the beating frequency for similar amplitudes are written alongside the theoretical values can be clearly seen in Table 4, and are restated in tabulated form below.

	$\frac{1}{2}A_{max}$ Comparison		$\frac{1}{3}A_{max}$ Comparison	
	Carrier Frequency (kHz)	Beating Frequency (kHz)	Carrier Frequency (kHz)	Beating Frequency (kHz)
Measured Value	40.11±0.01	1.39±0.01	39.47±0.01	0.53±0.01
Theoretical Value	40.48±0.01	1.43±0.01	39.48±0.01	0.58±0.01

As for the measured values with two waves of differing amplitude, the final results can be seen in Table 5, and are tabulated below:

	Experimentally measured data	Theoretical Value
f_m (kHz):	39.91±0.01	40.06±0.01
f_b beating frequency (kHz):	0.71±0.01	0.76±0.01

These results demonstrate that the carrier frequency of a superposed wave is often much larger than that of its beating frequency. In the real world, this phenomena is used for a process called modulation, where a wave of high frequency is 'modulated' to a lower frequency through the use of this phenomena. This technique is used in the real world in professions such as music, signal processing, and electrical engineering.

Another universally important aspect of sound measured during this experiment was its velocity. Below, the velocity of sound for two different setups is restated, each corresponding to its specific setup: acoustic plate and no acoustic plate.

$$v_{plate} = (357.56 \pm 6.9)[ms^{-1}]$$

$$v_{noplate} = (316.04 \pm 4.9)[ms^{-1}]$$

While these two values do not fully adhere to the theoretical value, they sufficiently demonstrate the range of velocities in which the velocity of sound in air lies. The speed of sound is an incredibly important physical constant, and is known to be approximately 343 m/s in 20 degree Celsius air (OpenStax, 2024).

Lastly, this investigation measured the diffraction patterns of ultrasound in air for a various number of slits. Diffraction is an important physical concept and is observed not only in sound but in all travelling waves. The results measured during the experiment sufficiently match that expected by the relevant theory–as discussed in the previous section–and provide insights into this property. Moving forward, the diffraction setup involving the rotary stage could be improved to minimize the aforementioned random errors introduced by the ambient conditions, the amplifier, and the acoustic impedance of the air between.

References

OpenStax. (2024). *17:3 speed of sound.* https://phys.libretexts.org/Bookshelves/University_Physics/University_Physics_(OpenStax)/Book%3A_University_Physics_I_-_Mechanics_Sound_Oscillations_and_Waves_(OpenStax)/17%3A_Sound/17.03%3A_Speed_of_Sound. LibreTexts.

Purves, D., Augustine, G. J., Fitzpatrick, D., et al. (2001). *Neuroscience* (2nd ed.). National Library of Medicine.

Wagner, V., & Söcker, T. J. (2024). Advanced physics lab 1 manual. *Constructor University*.

8 Appendix A

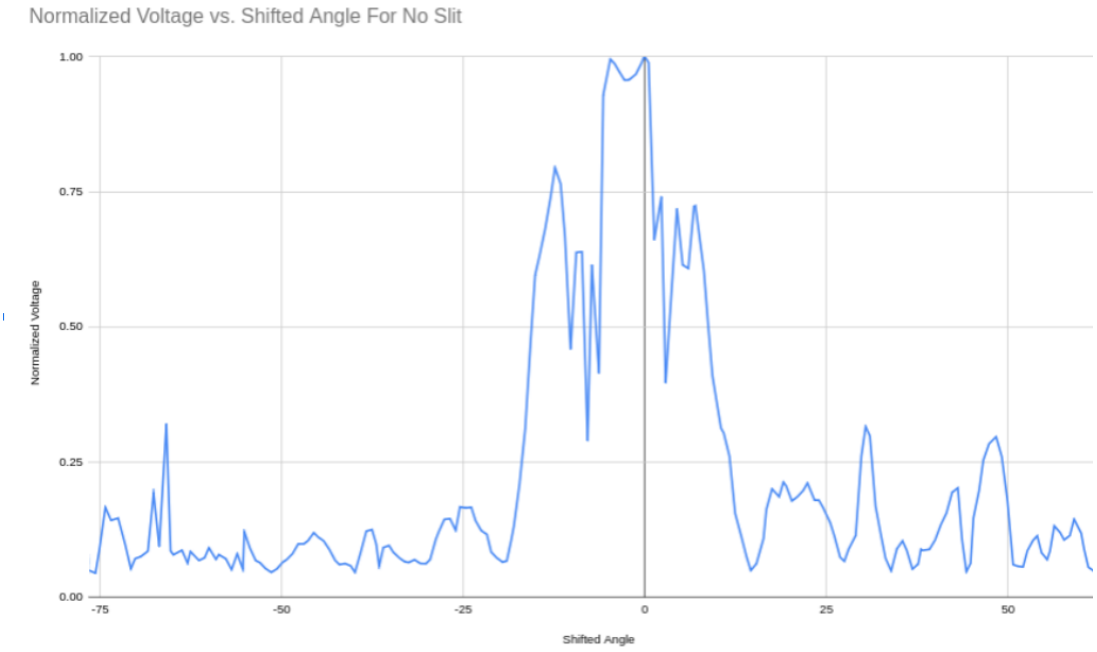

Figure 10: Plot of Normlalized Voltage (V) Against Rotation Angle (Deg) for 0 Slit

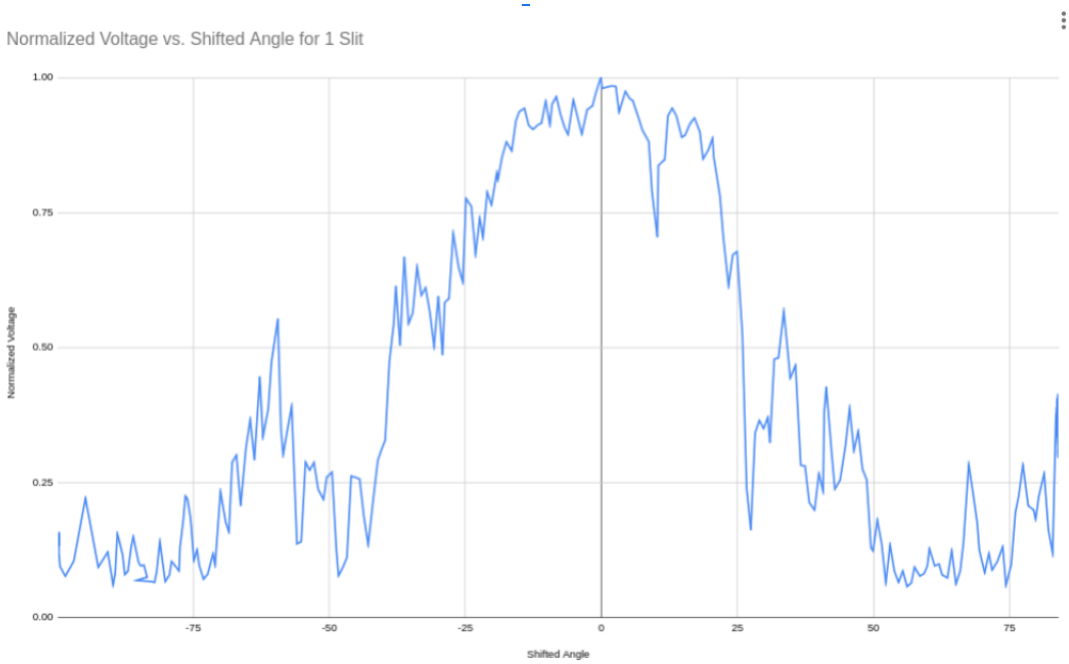

Figure 11: Plot of Normlalized Voltage (V) Against Rotation Angle (Deg) for 1 Slit

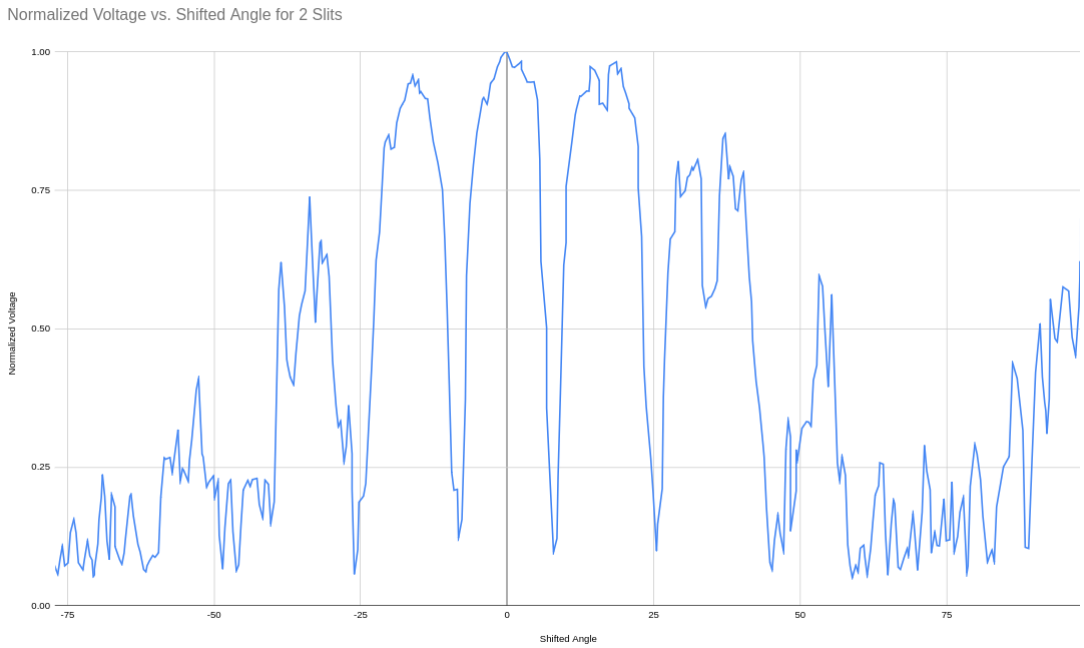

Figure 12: Plot of Normlalized Voltage (V) Against Rotation Angle (Deg) for 2 Slits

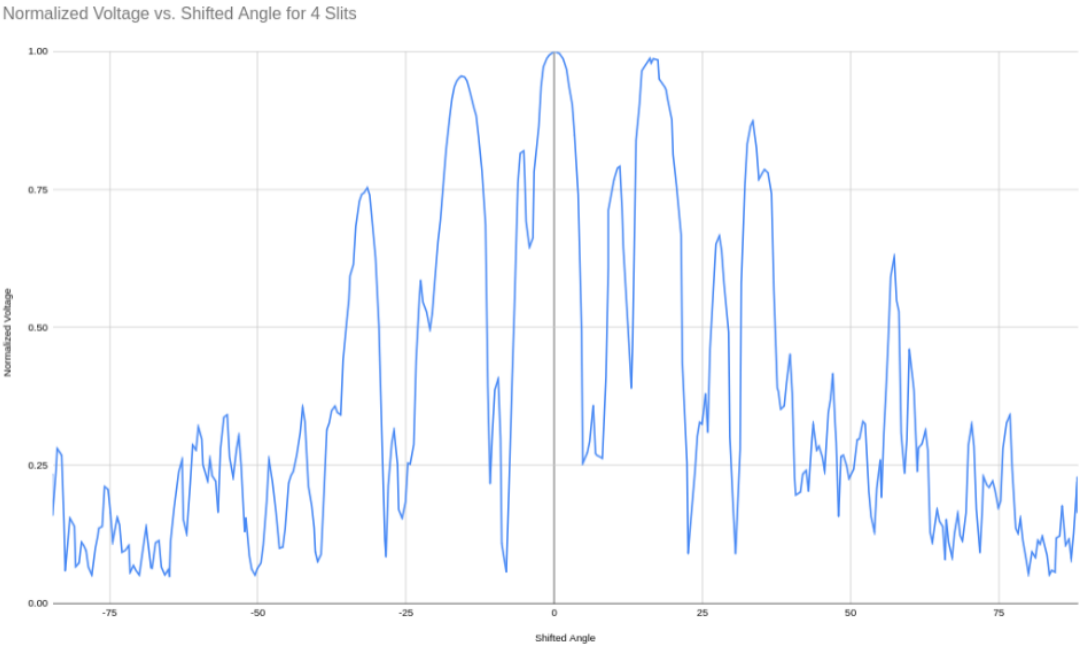

Figure 13: Plot of Normlalized Voltage (V) Against Rotation Angle (Deg) for 4 Slits

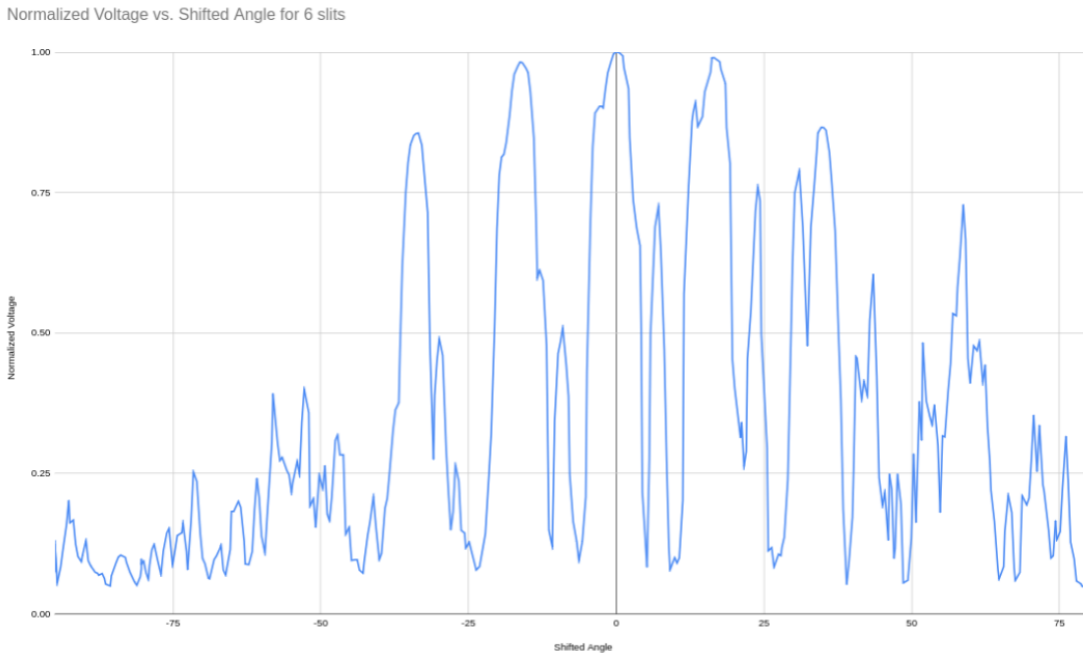

Figure 14: Plot of Normlalized Voltage (V) Against Rotation Angle (Deg) for 6 Slits

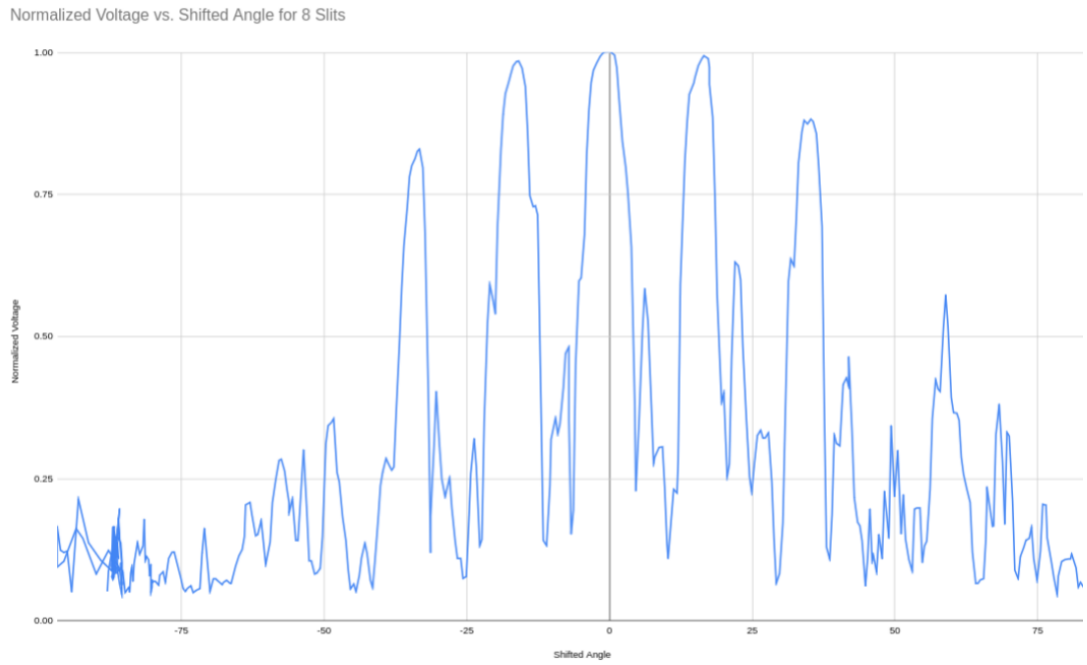

Figure 15: Plot of Normlalized Voltage (V) Against Rotation Angle (Deg) for 8 Slits

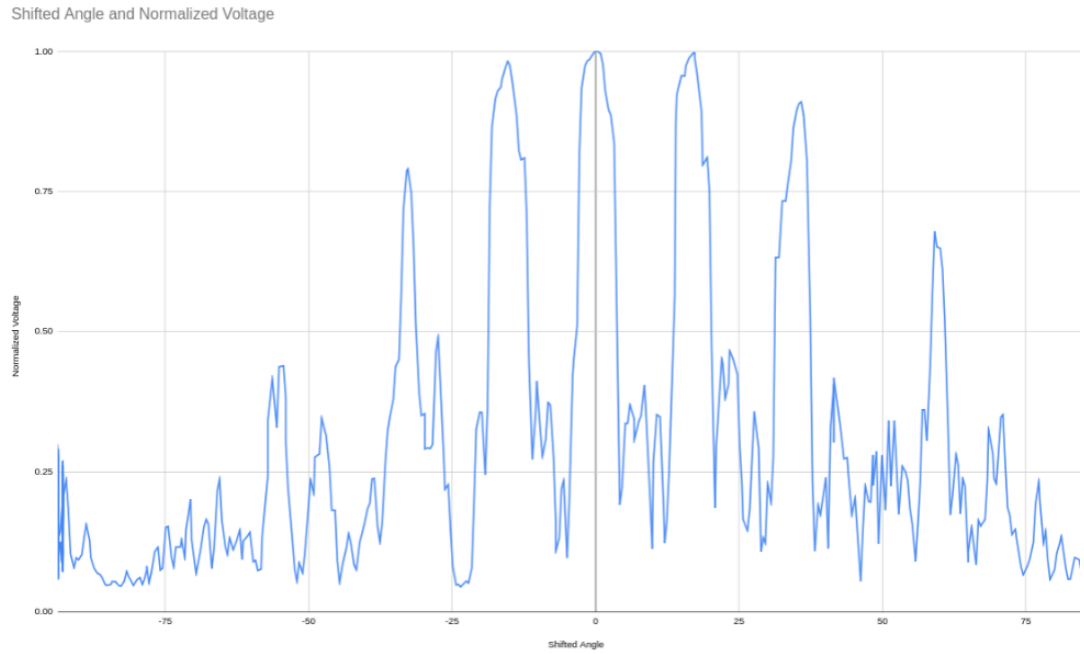

Figure 16: Plot of Normlalized Voltage (V) Against Rotation Angle (Deg) for 10 Slits

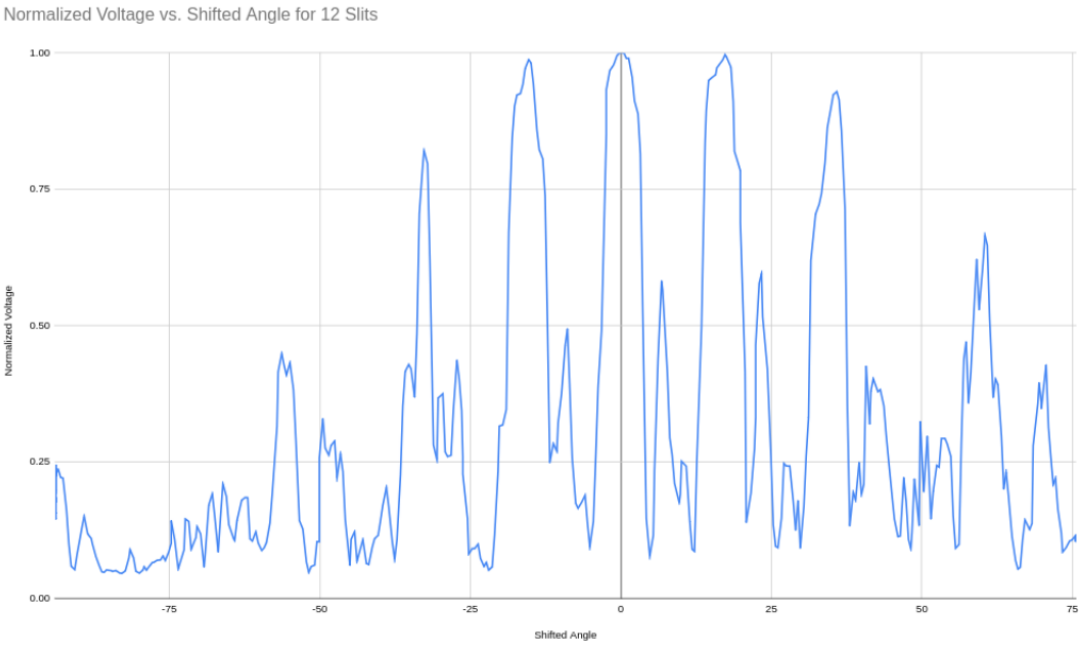

Figure 17: Plot of Normlalized Voltage (V) Against Rotation Angle (Deg) for 12 Slits

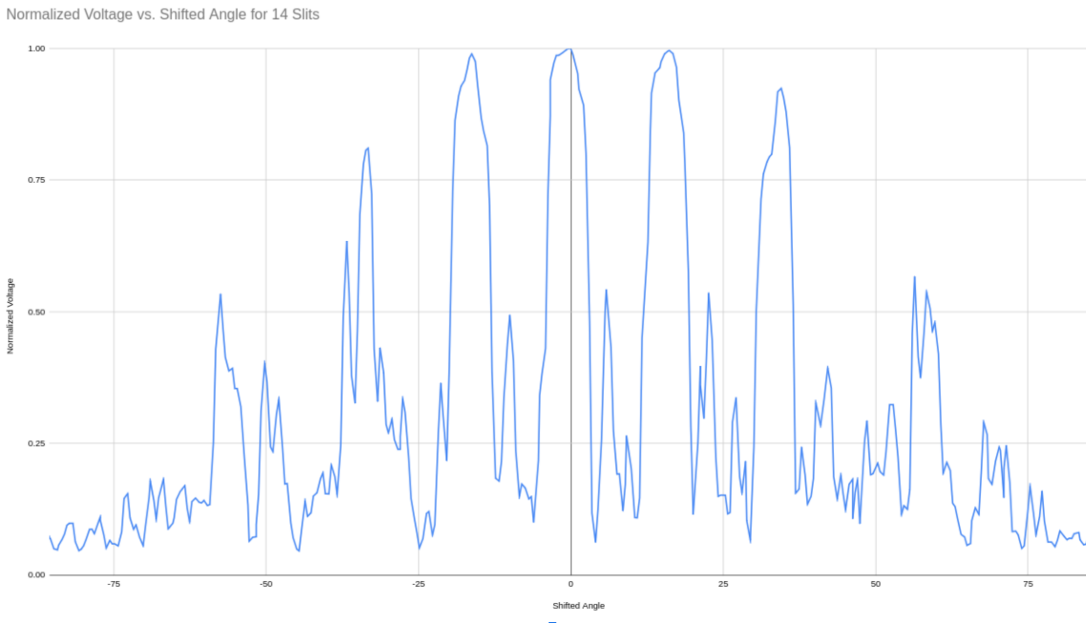

Figure 18: Plot of Normlalized Voltage (V) Against Rotation Angle (Deg) for 14 Slits